ACES Asian Chemical Editorial Society

doi.org/10.1002/asia.202101087

CHEMISTRY AN ASIAN JOURNAL Full Paper

Special Collection

Exploring the Role of Surface States in Emissive Carbon Nanodots: Analysis at Single-Particle Level

Dongseok Kim[+],[a] Rosemary L. Calabro[+],[b] Abdullah A. Masud[+],[b] Nadeesha L. Kothalawala,[b] Minsu Gu,[a, c] Seung-Yeon Kwak,[d] Won-Joon Son,[e] Kyu Young Hwang,[d] Hyeonho Choi,[d] Christopher I. Richards,*[b] Doo Young Kim,*[b] and Byeong-Su Kim*[a]

Abstract: Fluorescent carbon nanodots (CDs) have been highlighted as promising semiconducting materials due to their outstanding chemical and optical properties. However, the intrinsic heterogeneity of CDs has impeded a clear understanding of the mechanisms behind their photophysical properties. In this study, as-prepared CDs are fractionated via chromatography to reduce their structural and chemical heterogeneity and analyzed through ensemble and single-particle spectroscopies. Many single particles reveal fluorescence intensity fluctuations between two or more discrete levels with bi-exponential decays. While the intrinsic τ_1 components are uniform among single particles, the τ_2 components from molecule-like emissions spans a wider range of lifetimes, reflecting the inhomogeneity of the surface states. Furthermore, it is concluded that the relative population and chemical states of surface functional groups in CDs have a significant impact on emissive states, brightness, blinking, stability, and lifetime distribution of photoluminescence.

Introduction

Recent decades have witnessed the revolutionary development of semiconducting quantum dots (QDs), from laboratory-scale synthesis to actual products owing to their strong photoluminescence (PL), stability, and tunable photophysical properties.[1] Despite these advantages, environmental and health concerns associated with heavy metals present in QDs have limited further application. As a benign alternative to inorganic QDs, carbogenic nanoparticles (also known as carbon nanodots, CDs) have received considerable attention by virtue of their interesting physical, chemical, and optical properties, including facile preparation and functionalization, high solubility, and biocompatibility.[1c,2] These unique attributes have triggered the application of CDs in a wide array of fields, such as bioimaging, optoelectronics, photocatalysis, and optical sensing.[3]

Significant research efforts have been made to produce CDs with enhanced and controllable photophysical properties. This has led to the exploration of various synthetic methods and combinations of precursors. Despite recent progress, the miscellaneous collection of synthetic protocols often complicates the interpretation and optimization of the CD's photophysical properties; these can be strongly dictated by synthetic precursors, synthetic methods, and even purification or post-treatment.[4] Unlike the highly tunable and predictable photophysical properties of inorganic QDs, a clear mechanism of multi-color PL from CDs has not yet been ascertained. For example, quantum confinement effects, surface defects, emissive traps, edge and surface functional groups, and degree of surface passivation have all been proposed as the origin of PL in CDs.[5] The equivocal origin of PL poses a significant challenge for future development and application of CDs in various fields.

It is thus evident that in order to control the photophysical properties, it is critical to determine the origin of PL and, more importantly, to reduce the structural and chemical heterogeneity between individual CD particles in terms of size and chemical composition. However, there remains a question regarding the origin of the commonly observed excitation-dependent emission behavior of CDs.[6] In this context, single particle spectroscopy can offer unparalleled information regarding the photophysics of individual CD particles,[7] which cannot be typically observed in ensemble studies. For example, surface functional groups of CDs (e.g. oxygen and nitrogen functional groups) are commonly known to create low-energy emissive states, inducing red-shifted emission in ensemble measurements.[5b,8] In contrast, at a single-particle level, our

[a] D. Kim,[+] Dr. M. Gu, Prof. B.-S. Kim
Department of Chemistry, Yonsei University
Seoul 03722, (Republic of Korea)
E-mail: bskim19@yonsei.ac.kr

[b] Dr. R. L. Calabro,[+] A. A. Masud,[+] N. L. Kothalawala, Prof. C. I. Richards, Prof. D. Y. Kim
Department of Chemistry, University of Kentucky
505 Rose Street, Lexington, Kentucky 40506-0055 (United States)
E-mail: chris.richards@uky.edu
dooyoung.kim@uky.edu

[c] Dr. M. Gu
Department of Chemical Engineering (BK21 FOUR), Dong-A University
Busan 49315 (Republic of Korea)

[d] Dr. S.-Y. Kwak, Dr. K. Y. Hwang, Dr. H. Choi
Samsung Advanced Institute of Technology (SAIT), Samsung Electronics Co. Ltd.
Suwon 16678 (Republic of Korea)

[e] W.-J. Son
Data and Information Technology (DIT) Center, Samsung Electronics
Hwaseong 18448 (Republic of Korea)

[+] These authors contributed equally to this work.

Supporting information for this article is available on the WWW under https://doi.org/10.1002/asia.202101087

Special Collection This manuscript is part of a special collection celebrating the 75th Anniversary of the Korean Chemical Society.

previous work showed that oxygenated functional groups in CDs could contribute not only to low-energy emissive states but also traps or quenching states, resulting in a single-level photoblinking behavior.[9]

Meanwhile, unique redox events at the surface of CDs during photoexcitation were confirmed by the suppression of PL when electron donors or acceptors were in close proximity.[10] Based on single-particle analysis, it was determined that CDs were reversibly switched from a dark radical state to a bright state via an electron transfer process upon a brief exposure to blue light.[11] However, the relationship between the dark states and chemical functional groups of CDs remains unclear.

In this regard, we chose a well-known CD as a model system that possesses diverse surface states exhibiting multi-color emission and conducted an in-depth investigation via ensemble and single-particle analyses. To minimize the structural heterogeneity, as-synthesized CDs were fractionated via column chromatography. The polarity of CDs was identified as an important factor for determining the separation.[7b] Using confocal microscopy, fluorescence intensity time traces and lifetime decays were simultaneously recorded for single CD particles. Many individual CD particles exhibited fluorescence intensity fluctuations between two or more discrete levels, before they were photobleached. Particles were classified as exhibiting single-step photobleaching (no intermittency or blinking), single-level photoblinking, or multi-level fluctuations. Moreover, ensemble and single-particle spectroscopic analyses following fractionation confirmed that oxygenated groups in CDs constituted non-radiative decay channels and, more interestingly, that surface chemical states dramatically influenced emissive states with large in-homogeneity in PL behavior (Scheme 1).

Results and discussion

Carbon nanodots (CDs) often exhibit blue PL, attributed to the aromatic sp^2 carbon configuration in the core of the CDs contributing to their intrinsic state. For multi-color emissive CDs, a wide range of synthetic approaches with synthetic conditions, methods, and reagents have been reported to date.[1c] Among them, a combination of citric acid and urea was selected as a precursor for the solvothermal synthesis of CDs in this study.

The as-synthesized product was a mixture of CDs with a distribution of sizes and surface states, exhibiting broad absorption bands and full-color emissions contingent upon excitation wavelength (Figure 1a). Crude CDs were then separated via column chromatography to fractionate the sample based on surface oxidation state (Figure S1). Among the six different fractionated samples, three fractionated CDs were selected as representative fractions showing distinct photophysical properties, labelled F_A, F_B, and F_C depending on the elution time in column chromatographic separation. It should be noted that crude sample is not simply the sum of F_A, F_B, and F_C samples in this study since some residues of the crude sample are not eluted. The total reaction yields of each fractionated sample were measured by using simple weight ratio of precursors and CDs, leading to a significantly low yield after all, such as $F_A = 0.04\%$, $F_B = 0.23\%$, $F_C = 0.25\%$. Optical characterization of each fractionated sample was conducted via UV-vis and PL measurements (blue and red spectra for $\lambda_{ex} =$ 330 nm and $\lambda_{ex} = 540$ nm, respectively) (Figure 1b–d). All fractionated samples shared common absorption bands in the UV region assigned to the π–π^* transition of the sp^2-carbon core. However, each sample exhibited distinct absorption bands between 310 and 660 nm, reflecting the presence of different surface states. While F_A showed dominant blue emission, both

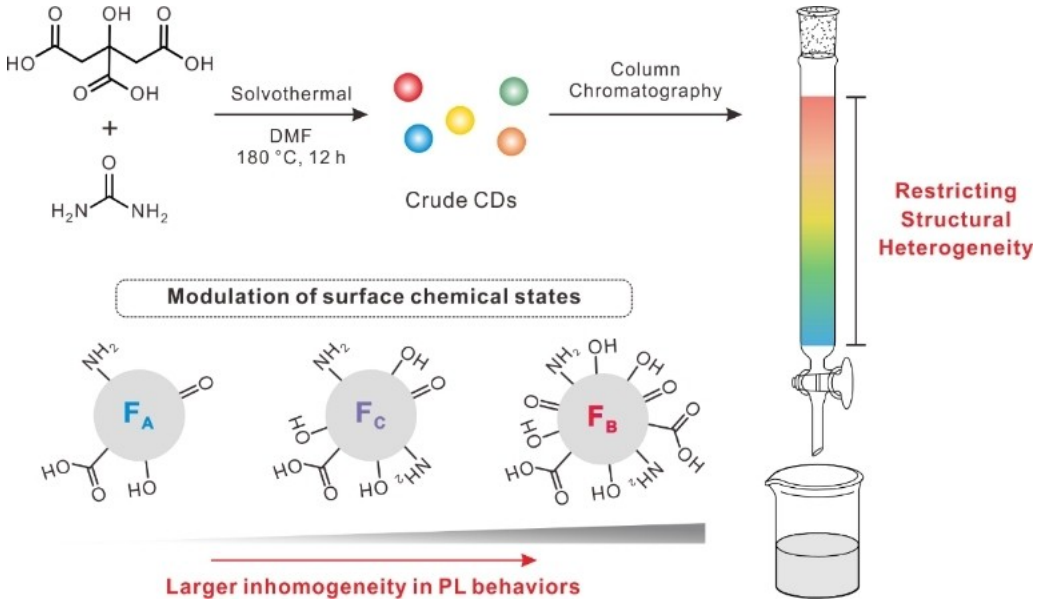

Scheme 1. Solvothermal synthesis and fractionation of CDs to restrict structural heterogeneity of CDs and their corresponding PL behaviors depending on the surface chemical states.

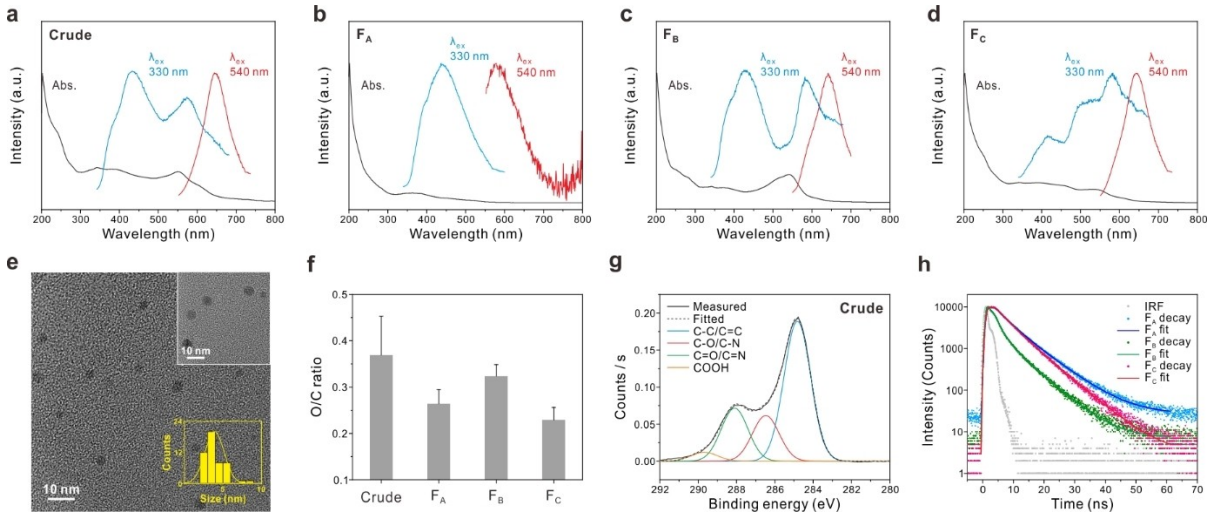

Figure 1. Characterization of fractionated CDs. (a–d) Normalized absorbance and emission spectra for a) crude and each fractionated CD: b) F_A, c) F_B, and d) F_C. Note that F_A shows immensely weak emission at 540 nm excitation as indicated by its noisy spectrum. (e) Representative TEM images of crude CD with a size distribution histogram. (f) O/C ratio of each CD obtained from XPS spectra. (g) Deconvoluted high-resolution XPS spectra of crude CD for C1s. (h) PL decay profile from ensemble time-correlated single photon counting (TCSPC) measurements for each fractionated CD ($\lambda_{ex}=455$ nm and $\lambda_{em}=575$ nm).

F_B and F_C contained significant red emissive states when excited at a longer wavelength of 540 nm, resulting from several low-energy n–π* transition states.

The quasi-spherical morphology of crude CDs was characterized using transmission electron microscopy (TEM), showing an average diameter of 3.91 ± 1.24 nm (Figure 1e). It should be noted that the average size of each fractionated CD was relatively uniform across all samples (Figure S2, F_A: 2.73 ± 0.80 nm; F_B: 3.07 ± 0.63 nm; and F_C: 2.90 ± 0.74 nm) as the separation of the CD was dependent primarily on surface oxidation state and polarity, regardless of size. The discrepancy in the size of particles is attributable to that there are still some fractions not eluted from the column chromatography. X-ray photoelectron spectroscopy (XPS) was used to verify the degree of surface oxidation and chemical composition of each fraction. The four samples mainly comprised of C, N, and O, with different atomic ratios (Table S1). High-resolution C1s, N1s, and O1s XPS spectra, for the crude CDs and each fractionate, are shown in Figure S3–S5 and their chemical states are summarized in Table S2–S4. Because there was no noticeable difference in the sizes of CD fractions, the polarity of each fraction is likely to be a primary factor to determine the order of fractionates in chromatographic separation. Surprisingly, the F_B sample contained higher content of oxygen and nitrogen than F_A and F_C samples (Figure 1f and Figure S6). FT-IR spectra of each fractionated CDs also proved that there is relatively higher fraction of oxygenated group, especially O–H group, in the fractionated sample compared to crude CDs, which corresponds to the results from XPS (Figure S7). In addition, C–H stretching peak (2966–2863 cm^{-1}) significantly observed in the fractionated samples indicate the presence of aliphatic chains present in fractionated CD. This observation also supports that a large amount of residue initially present in the crude CDs was not eluted in the column chromatography due to their high polarity. A mismatch between the overall contents of oxygen and nitrogen and the separation order suggested that additional factors may play a role in the chromatographic separation. Some possibilities can be proposed; 1) in addition to the overall oxygen content, the actual structures associated with oxygenated groups and their locations of oxygenated groups in CDs may influence the polarity and the separation and 2) due to high contents of pyrrolic and carboxylic acid groups in F_C compared to F_B, electrostatic interactions as well as hydrogen bonding with the silica-gel stationary phase could delay the elution time of F_C. However, further investigations are necessary to explore the proposed possibilities and this will be the subject of our on-going efforts.

The deconvoluted high-resolution XPS C1s spectra of crude (Figure 1g) and fractionated CDs revealed that the composition was significantly different depending on the type of fractionate. For example, the C–C/C=C (284.7 eV), C–O/C–N (286.5 eV), C=O/C=N (288.1 eV), and COOH (289.7 eV) could be identified (Figure S3). The F_B sample contained a high proportion of C–O/C–N and C=O/C=N groups (Table S2). Notably, it has been claimed that the C=O or C=N groups create triplet states that played an important role in non-radiative vibrational and rotational decay pathways.[12] In all fractionates, the majority of nitrogen atoms were found at the edges in the form of either pyridinic-N or pyrrolic-N; there was only a low content, if any, of graphitic-N, which was internalized to the sp^2-domain of the carbonaceous core. No graphitic-N was observed in the F_B CDs. It is known that pyridinic-N or graphitic-N, conjugated with the π system, can enhance the brightness and PL quantum yield of CDs.[13] The absorption and PL spectra results indicate the successful separation of each of the fractionated CDs, depending on the degree of surface states.

PL quantum yields for each sample were determined at the excitation wavelength, obtaining the highest steady-state PL ($\lambda_{ex}=390$ nm for F_A and F_B, $\lambda_{ex}=450$ nm for F_C) (Table S5). F_A had the highest quantum yield of 22%, while F_B and F_C had

lower quantum yields of 4.5% and 18.5%, respectively. Ensemble PL decay curves of F_A, F_B, and F_C, recorded via time-correlated single photon counting (TCSPC) measurements (λ_{ex} = 455 nm and λ_{em} = 575 nm) and their fittings are presented in Figure 1h and these parameters are summarized in Table S6. The PL decay curves were recorded at emission wavelengths of 630 nm (Figure S8) and the determined fitting parameters are summarized in Table S7. All samples were best fit using three exponential decay functions, in accordance with previous reports.[14] The fast τ_1 component (0.31–0.49 ns) was assigned to intrinsic emissions associated with the sp^2-domains within the particle[15] and the slower τ_2 (1.7–4.1 ns) and τ_3 (6.5–7.9 ns) components were assigned to various functional groups, with the intermediate τ_2 component typically associated with chemically reduced states and the slower τ_3 component with more oxidized states.[6b,16] The τ_1 component was more uniform across all three fractionates, implying the intrinsic states are similar among these samples. However, the relative contribution of the intrinsic τ_1 emission for sample F_B (21%) was significantly higher compared to that of F_A and F_C (only 3–4%). The τ_2 and τ_3 component contributed the most significantly to both F_A and F_C and was slightly slower for both samples than that observed with sample F_B. When comparing the three samples, it is not surprising that samples F_A and F_C had similar ensemble behaviors, since their C- and N- configurations (Table S2 and Table S3), both in atomic percentages and distribution of functional groups, exhibited more similarities with each other than with F_B, according to the XPS data.

The single-particle experimental set-up used in this study is shown as a schematic diagram (Figure 2a). Fluorescence intensity decay profiles and time-dependent intensity fluctuations of single CD particles were simultaneously collected via a TCSPC unit and an avalanche photodiode (APD), respectively. CD particles from either F_B or F_C were dispersed and embedded in a poly(vinyl alcohol) (PVA) film. In these PVA films, a particle-particle distance between CDs was sufficient for resolving individual particles. It should be noted that only F_B and F_C samples were examined for single-particle analysis, since the excitation wavelength for F_A (330 nm) generates high background signals from the optics. The single-particle fluorescence images of samples F_B and F_C are shown in Figure 2b and 2c, respectively. For reference, an image of the PVA film is shown in

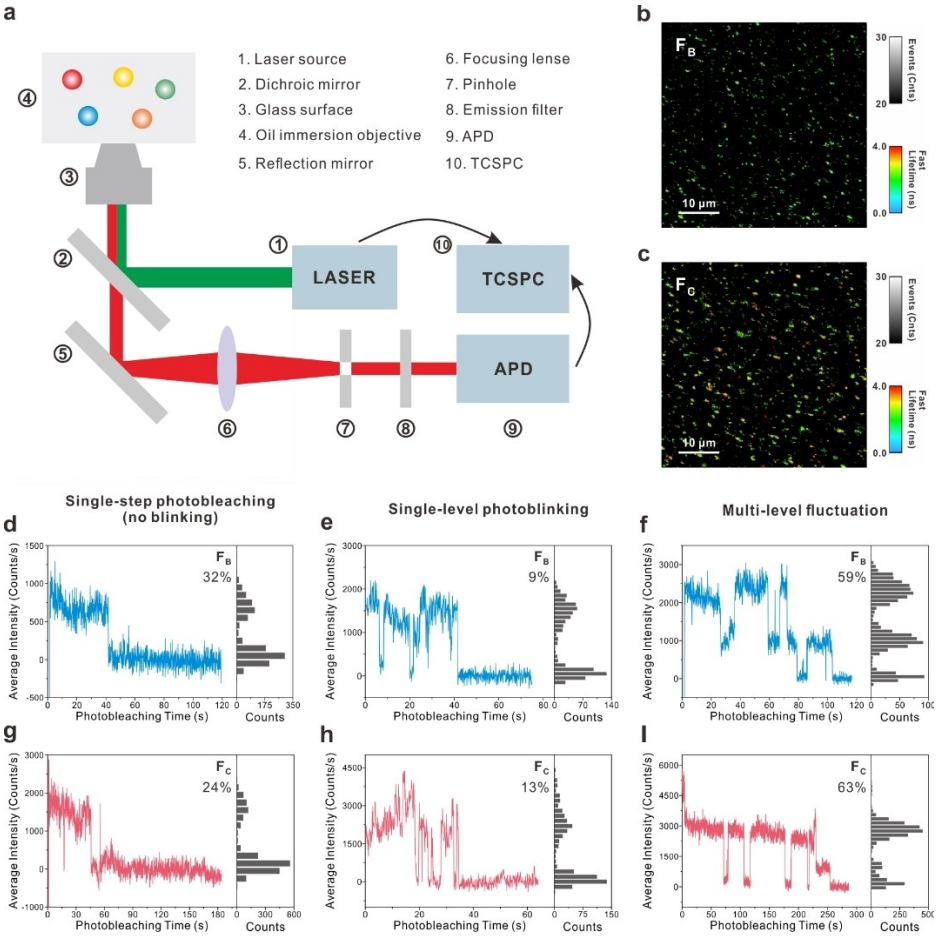

Figure 2. Single-particle fluorescence studies of F_B and F_C. (a) A schematic diagram of a confocal microscopic set-up for single-particle analysis. (b, c) Single-particle fluorescence images of samples F_B and F_C. The fluorescence intensity and lifetime of individual CD particles is indicated by the vertical bar located at the top and colored vertical bar located at the bottom, respectively, in each image. (d–i) Single-particle fluorescence time traces of samples F_B and F_C classified into three behaviors, including single-step photobleaching (no blinking), single-level photoblinking, and multi-level fluctuation. The value in each graph is the percentile of particles showing the specific fluorescence behavior. Each graph shows the representative PL intensity fluctuation of a single particle (left panel) with the corresponding intensity histogram (right panel). Background intensity (Raman signal from PVA) was subtracted from the counts in Figure 2d-i.

Figure S9. Overall, the particles in sample F_C are much brighter and have longer lifetimes than particles in sample F_B, implying the high population of bright emissive states in F_C.

Representative fluorescence intensity transients over time of single particles from F_B (Figure 2d–f) and F_C (Figure 2g–i) are presented (see Table S8). The majority of CD particles exhibited fluorescence fluctuations between two or more discrete intensity levels. The behavior of particles was classified into three categories: (i) single-step photobleaching with no blinking or intermittency, (ii) single-level photoblinking, and (iii) multi-level fluctuations. About one third of the particles in F_B and F_C showed either single-step photobleaching (Figure 2d and 2 g) or single-level photoblinking behavior (Figure 2e and 2 h), implying the presence of single chromophores in individual CD particles, which could be excited. As shown in Figure 2d and 2 g, the fluorescence intensity remained constant until the particles became photobleached. In photobleaching, the particles were permanently transformed to a non- or less-emissive state.[17] Figure 2e and 2 h show a single-level photoblinking behavior with reversible emission transition between on- and off-states, before the particles were photobleached. The majority of the particles in both F_B and F_C exhibited intensity fluctuations between multiple discrete levels (59% for F_B and 63% for F_C), reflecting the presence of multiple chromophoric units in single particles (Figure. 2f and 2i). The presence of multiple chromophores at different energy states is unquestionably one source of the inhomogeneous and excitation-dependent emissions commonly reported in ensemble studies.

The single-level photoblinking or multi-level intensity fluctuation is due to the transition from a bright (emissive) state to a dark (less or non-emissive) state under excitation.[18] A possible origin of the dark states in these CDs includes long-lived triplet states generated by inter-system crossing from initially photo-excited singlet states associated with surface C=O and C=N groups,[12] reversible meta-stable excited states, or thermally induced changes to the electronic ground state.[17] A further possibility in this study could be the formation of radical ions due to reactive hydroxyl groups in the PVA matrix interacting with surrounding functional groups of CDs.[18] Thus, the radical ions formed serve as dark states which can possibly relax back to the ground state.

Figure S10 presents histograms of the photobleaching times, determined for individual particles sampled in F_B and F_C, which were fit to single exponential decay curves. The fluorescence intensity histograms of single particles exhibited single- and multi-level photobleaching for F_B and F_C (Figure S11). It can clearly be seen that F_B has a faster photobleaching time than F_C, indicating that the CD particles in F_C are more resistant to photobleaching than those in F_B. Meanwhile, particles in F_C showed both higher and a wider range of fluorescence intensities than particles in F_B. The difference in photostability and brightness of the two samples can be related to the differences in chemical composition. According to the XPS data (Figure 1 and Table S2–S4), individual particles in sample F_C have a lower O/C ratio and a higher content of graphitic or pyridinic nitrogen, which improves photostability and increases the PL quantum yield. They generate more emissive states (molecule-like emission) than intrinsic states;[5a,d] this is consistent with the predominant contribution of τ_2 and τ_3 components in F_c observed in ensemble TCSPC measurements (Table S6 and S7).

TCSPC of the individual particles in F_B and F_C was also determined, as shown in Figure 3. Unlike the ensemble TCSPC where the decay curves were best fit using three exponentials, all the individual particles were fit with either single- (Figure 3a) or bi-exponential decays (Figure 3b). While a substantial number of particles exhibited single-exponential decay behavior, implying single chromophore emission, a majority of the particles in both samples exhibited bi-exponential decays (84% for F_B and 65% for F_C), indicating that individual particles possess both faster intrinsic and slower extrinsic emissive states. Figure 3c and Figure 3d present the histograms of lifetimes with single exponential decay (τ) and bi-exponential decay (τ_1 and τ_2) in the samples F_B and F_C, respectively. For the particles showing bi-exponential decay, the intrinsic τ_1 component was surprisingly uniform (~0.5 ns) across all particles, with a similar value as observed from the ensemble measurements (0.31–0.49 ns). In contrast, the τ_2 component was much more widely distributed, reflecting the structural and chemical heterogeneity of surface states present in each sample. The distribution of the single-particle τ_2 was consistent with that of the τ_2 determined via the ensemble TCSPC measurements. The samples that were fit to a single-exponential decay also showed a broad distribution, suggesting that their main deactivation pathway is associated with oxygenated functional groups. Notably, neither F_B nor F_C had any particles with tri-exponential behavior. A possible explanation for the absence of the longer τ_3 lifetime is that it is either merged with the τ_2 component, due to the PVA matrix environment, or it is not bright enough to be detected at the single-particle level.[19] Additionally, the hydroxyl groups from the PVA matrix can quench the PL of single CD particles via hydrogen bonding with oxygenated groups of CDs.[18] In this case, PL quenching is more probable for the longer lived τ_3, which is typically associated with highly oxygenated functional groups.[6b]

For the single particles exhibiting bi-exponential behavior, the distribution of fluorescence intensity vs. lifetime was determined for F_B and F_C (Figure 3e and 3f). In general, most of the τ_2 components had a higher intensity than the τ_1 components (94% of particles for F_B and 91% of particles for F_C) indicating that the τ_2 emission is a bright state. A much larger fraction of τ_2 components in F_C exhibited higher intensities of >150 kcounts, indicating that more bright states are present in F_C. This is consistent with the higher PL quantum yield of F_C (18.5%) than of F_B (4.5%) determined in the ensemble measurements. Figure S12 presents plots of the same lifetime intensity vs. lifetime distribution with the particles exhibiting single-level fluctuations separated from those showing multi-level fluctuations. For both F_B and F_C, the particles with a single-level fluctuation generally exhibited lower intensities, whereas the particles showing higher intensities exhibited multi-level fluctuations. This can be explained by the fact that these particles are likely to have multiple bright chromophoric units that contribute to the emission. If we consider the relative intensities of

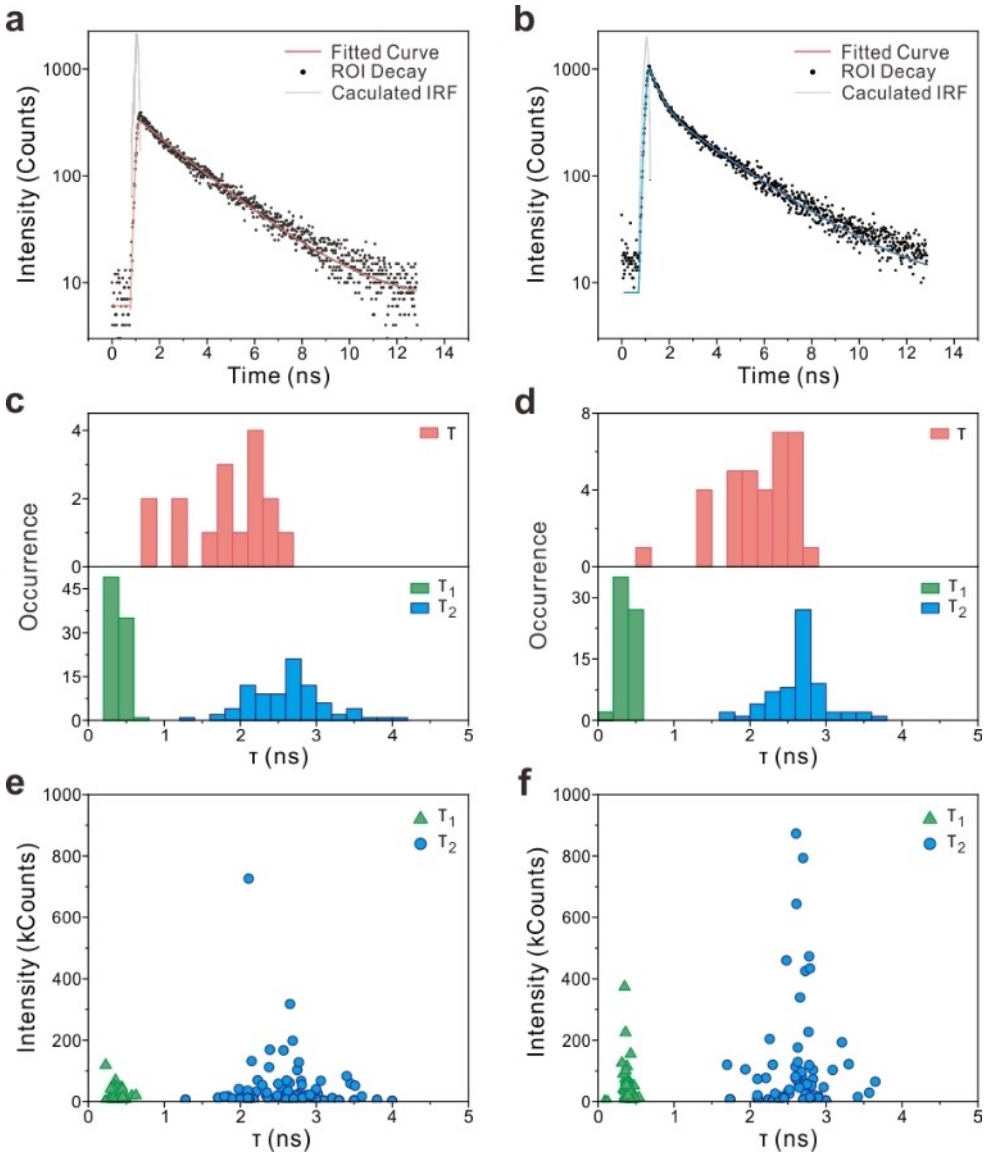

Figure 3. Selected TCSPC decay curves obtained from single-particle measurements showing (a) single exponential decay and (b) bi-exponential decay. Histograms of the single-particle fluorescence lifetimes for (c) F_B and (d) Fc, each of which is divided into two groups showing single exponential decay (τ) in the top panel and bi-exponential decay (τ_1 and τ_2) in the bottom panel. TCSPC lifetime intensity *vs.* lifetime plots for all measured particles in samples (e) F_B and (f) F_C.

these particles rather than the absolute intensities (Figure S13), it is clear that for all particles the molecule-like τ_2 component generally has a higher relative contribution than the intrinsic τ_1 component, indicating that the molecule-like τ_2 chromophore is a brighter emitting species than the intrinsic τ_1 chromophore.

Finally, we investigated how the lifetime of individual particles evolves during fluorescence intermittency. The transient intensity plot for a particle from sample F_B (Figure 4a) and F_C (Figure 4b) that exhibited multi-level discrete fluctuations was inspected and various regions of interest was highlighted with single-particle lifetime decay curves which were collected simultaneously at four regions of the fluorescence transients. In addition, the lifetime τ_1 and τ_2 components and their percentiles are determined for each of the decay curves. Table S9 and Table S10 present the lifetime fit parameters for the temporal regions of the fluorescence transients of individual CDs. Interestingly, we figured out that τ_2 components in both F_B and F_C samples were highly susceptible during fluorescence intermittency, changing in the emissive states or photophysical pathways related with surface states of individual particle. In region 1 of F_B, where the intensity is highest, the τ_2 contribution is 93.7%; the highest fraction observed among all the regions. In region 2, the emission intensity decreases, and the τ_2 contribution decreases to 84.3%. This implies that the molecule-like τ_2 chromophoric unit becomes darker in this region due to its partial transition to a dark state. The contribution from the τ_2 continues to decrease to 69.6% as the particle blinks on and off, until the CD particle is completely photobleached. Whereas τ_2 contribution in F_C decreases to only 82.0% in region 4. It means that the chemical states of individual CDs have significant

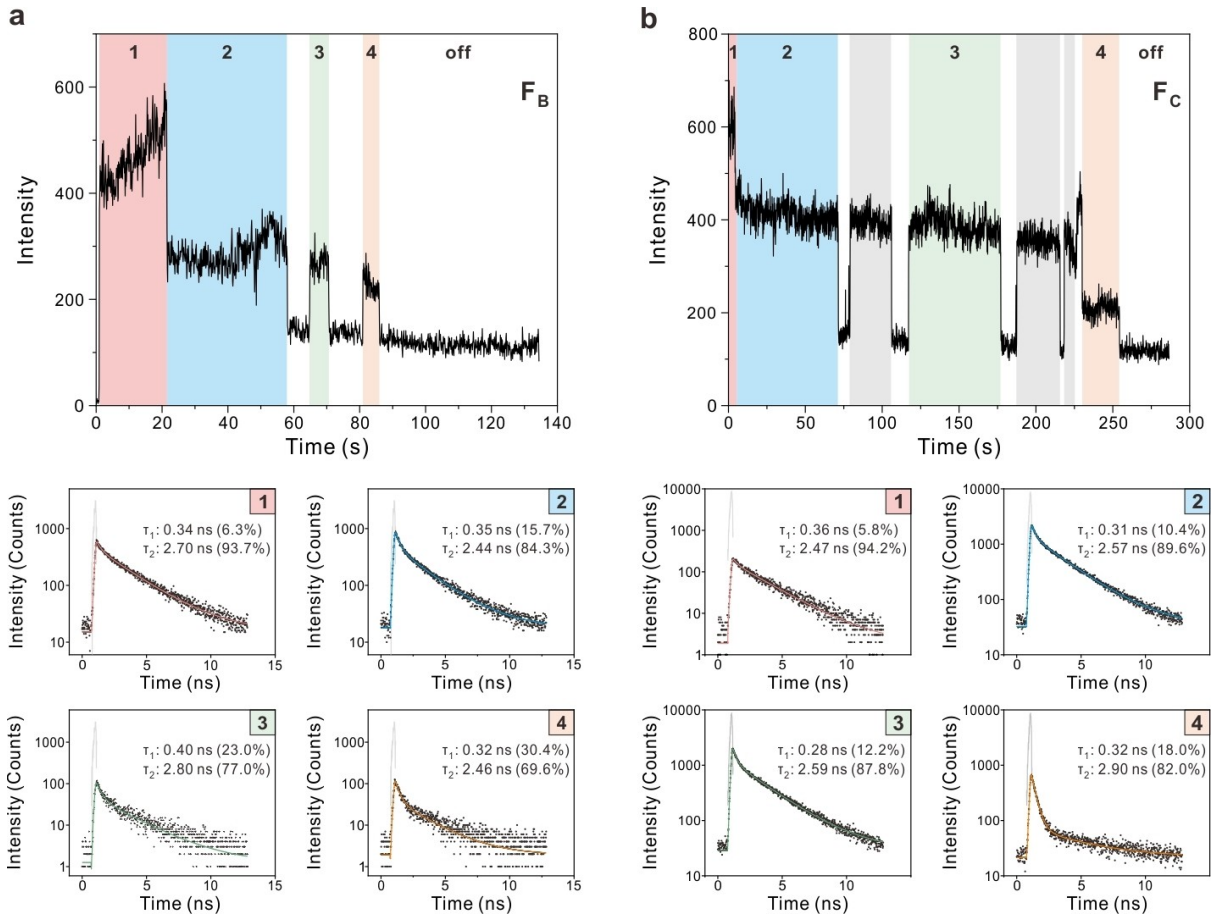

Figure 4. A fluorescence transient of a single CD particle exhibiting multiple discrete levels and four TCSPC decays recorded at various regions of the fluorescence transient from (a) F_B and (b) F_C. Note that the number in the fluorescence transient graph indicates the specific region in TCSPC decay curves.

impacts on the changes in emissive states during fluorescence intermittency with ensuing a large inhomogeneity in PL behavior. Moreover, unlike τ_1 component which remains constant within the margin of uncertainty, τ_2 component is more susceptible to photobleaching or photochemical reaction.

The precise origins for the higher susceptibility of τ_2 components are yet to be fully determined; as a possible mechanism for this partial transition to the dark state, we propose the oxidation of hydroquinone groups on the surface to benzoquinone during blinking under the absorption of light radiation,[20] as the carbonyl groups (possessing mixed n–π* and π–π* configurations) resulted in a higher intersystem crossing with long-lived triplet states (Figure S14).[12b] The contribution from the τ_2 component decreases with each bleaching or blinking step, suggesting the molecule-like chromophores attributed to the chemical states of CDs are more sensitive to photochemical reactions than intrinsic components.

Several important findings were made from the single-particle analysis. 1) In both F_B and Fc, individual particles possess multiple emissive species. 2) In both F_B and F_C, the τ_1 intrinsic chromophores are more uniform than the τ_2 chromophores originating from the surface states. This is largely due to in-homogeneity in the lower-energy emissive states due to the diverse functional groups. 3) The difference in surface chemical states (e.g. oxygenated and N-chemical states) between F_B and F_C had a significant impact on the single-particle PL behavior of CDs, such as brightness, blinking, stability, and lifetime distribution. These findings enable to further understand the complex nature of CDs, however, it should be noted that the inherent heterogeneity in CDs cannot be resolved simply by separating more fractions through column chromatography,[21] which warrants the importance of single-particle analysis employed in this study.

To obtain additional insights for the effect of surface chemical states in photophysical properties of CDs, surface activity of CDs toward an electron transfer process was investigated using the photocatalytic redox activity of CDs for generating active oxygen species.[22] As an alternative pathway to PL, photocatalytic reactions on the surface of CDs occur through serial events, including light absorption, exciton separation, and transport of electron and holes to the surface, followed by the desired photochemical reactions. It is thus suggested that the surface functional groups of CDs have a critical role in photocatalytic activity. Using methylene blue (MB) as a model compound, the photocatalytic degradation was monitored for each fractionated CD under visible light irradiation (Figure S15). Intriguingly, sample F_B shows the highest photocatalytic activity for the degradation of MB over 80%,

within 1 h. In contrast, both F_A and F_C showed lower activity. In addition, a trade-off relationship between photocatalytic activity and PL was observed; higher photocatalytic activity and a lower PL lifetime were observed in F_B, which possesses higher surface oxidation states (Figure S15c).

Considering competition between non-radiative decay through oxygenated defect and photocatalysis, it is possible that the higher electron affinity of oxygenated groups transferred photogenerated electrons from the neighboring aromatic domains toward the surface of the CDs, for the efficient degradation of MB (Figure S15d).[23] Furthermore, hydroxyl and amine groups on the surface act as an internal hole scavenger, helping the migration of photoexcited electrons and facilitating charge separation with higher photocatalytic activity.[23a,24] This result offers a valuable insight into the role of the CD's functional groups regarding charge carrier dynamics. Consequently, the lower proportion of graphitic and pyridinic nitrogen components and higher proportion of other functional groups in F_B resulted in a short excited-state lifetime of the CDs with dominant non-radiative decay pathways, involving not only vibrational decay, but electron transfer processes of the CDs in particular (Figure S15d). In this context, the transfer of photoelectrons to lower-energy surface states upon light irradiation can lead to irreversible photochemical change of the CDs, such as photobleaching of PL and photocatalytic reduction reactions at the surface. For future development and applications, it is noteworthy that the aforementioned electron transfer process in CDs offers new insight into the origin of the complicated photophysical properties of CDs.

Conclusion

In summary, we separated the multi-color emissive CDs using column chromatography and carried out ensemble and single-particle spectroscopic studies to understand the equivocal mechanisms of photoluminescence in terms of the surface chemical states of CDs. Through a fractionation process, the structural and chemical in-homogeneity of CDs was finely controlled and probed via spectroscopy, both at an ensemble and single-particle level. Consequently, two fluorescence decay components, τ_1 and τ_2, which indicate intrinsic and molecule-like emission, respectively, were resolved at a single-particle level. Owing to the restricted structural heterogeneity of CDs, the intrinsic τ_1 components showed a remarkably uniform behavior. In contrast, the τ_2 components varied with respect to various functional groups on the surface of CDs. It was concluded that the photophysical behavior of CDs (e.g. brightness, blinking, stability, and lifetime) were strongly affected by surface chemical states of CDs. In addition, we found that these surface emissive states were also inversely correlated with the electron transfer processes of CDs, as verified by the photocatalytic activity of each CD. We believe that these results can provide unique insights, not only for understanding the photophysical properties of CDs, but also for designing CDs toward prospective optical and electronic devices.

Experimental Section

Synthesis of carbon dots (CDs)

The CDs were prepared according to a previous report with some modifications.[25] Briefly, citric acid (1.34 g, 7 mmol) was dissolved in 10 mL of DMF. Then, 0.60 g of urea (10 mmol) was added into the solution, followed by solvothermal reaction at 180 °C for 12 h in a sealed Teflon-lined autoclave. After cooling to room temperature, the reaction mixture was poured into 200 mL of ethyl acetate and centrifuged at 9000 rpm for 10 min to obtain a dark brown precipitate. To remove remaining fluorescent impurities completely, the centrifugation was repeated over 10 times, with a mixture of ethyl acetate and methanol. The resulting black product was fractionated via silica column chromatography with gradient elution (dichlormethane:methanol (100:0 to 90:10, v/v)). The fractionated CDs were named as F_A, F_B, and F_C, depending on elution time.

Material characterizations

The absorbance and photoluminescence of each of the fractionated CDs were characterized using a UV-1800 UV/vis spectrophotometer and a RF-6000 spectrofluorophotometer (Shimadzu, Japan), respectively. High-resolution TEM (HR-TEM) imaging was conducted in the bright-field mode, using a JEM-F200 (JEOL, Japan). The analysis of chemical states was conducted using a K-alpha X-ray photoelectron spectroscope (XPS, Thermo-Fisher, USA).

Absolute quantum yield measurements

Absolute photoluminescence quantum yield (PLQY) measurements were performed with a Horiba Scientific fluorescence spectrometer (Fluoromax Plus-C) equipped with an integrating sphere. Samples were dissolved in methanol and excited at the wavelength that allowed maximum emission (390 nm for F_A and F_B and 450 nm for F_C) with 0.55 nm slits and a 5 s integration time. The emission was scanned in a spectral range to contain both the Rayleigh scattering peak of the excitation and the PL from the sample. A blank of the methanol solvent was also scanned in the same measurement ranges. PLQY was calculated based on the following equation: $\mathrm{PLQY} = \frac{P_B - P_A}{L_A - L_B} \times 100\%$, where P_B (P_A) refers to the integrated intensity of the sample (blank) in the PL emission range, and L_B (L_A) refers to the integrated intensity of the Rayleigh scattering of the sample (blank) in the excitation range. All PLQY calculations were made using the Horiba Scientific FluorEssence™ software and incorporated a factory-acquired integrating sphere correction.

Ensemble time-correlated single photon counting measurements

PL lifetime measurements were performed on a Horiba Scientific Fluoromax Plus-C equipped with a DeltaHub™ high throughput TCSPC controller and a NanoLED 455 pulsed excitation source. TCSPC results were collected at 575 and 630 nm emission with a bandpass of 5 nm, a repetition rate of 1 MHz, and a measurement range of 200 ns. The scattering of the excitation wavelength by a Ludox solution was measured to determine the instrument response function (IRF). The lifetime fits were obtained using the Horiba Scientific Decay Analysis Software DAS6. The TCSPC decays were fit to three-exponentials, in the form: $y = A + B_1 e^{-t/\tau_1} + B_2 e^{-t/3} + B_3 e^{-t/\tau_3}$ where A is a constant, B_n is a pre-exponential, and τ_n is the lifetime for the n^{th} term. The relative contributions for each lifetime were determined by the equation:

$$\%\tau_n = 100 \times \frac{B_n\tau_n}{B_1\tau_1 + B_2\tau_2 + B_3\tau_3}.$$

Single particle measurements

For samples F_B and F_C, a 5×10^{-5} mg/mL solution of CDs was mixed with 44 mg/mL of PVA. Glass coverslips (22×22 mm^2, #1.5) were cleaned to remove any photoluminescent contaminants by sonicating in a 5 M NaOH solution for 1 h at 45 °C, followed by 1 h sonication in 0.1 M HCl at the same temperature. The coverslips were rinsed with ethanol and DI water, air dried, and subsequently plasma cleaned for 4 min. Cleaned glass coverslips were attached to petri dishes using UV-reactive adhesive. The CDs were then immobilized on the glass cover slips by spin casting a 200 μL aliquot of CD solutions at 2000 rpm for 45 s. Single molecule TCSPC measurements were performed using a custom-built confocal microscopy setup equipped with an Olympus IX 83 inverted microscope. The glass coverslips with CDs immobilized on the surface were placed on a piezoelectric stage mounted on the microscope and raster scanned with a 532 nm confocal beam to image the particles. The confocal beam was produced from a SuperK extreme super-continuum pulsed laser and focused on the glass coverslip surface with an Olympus 60x, 1.45 NA oil immersion objective. Prior to exposure, the beam was filtered through a ZET 532/10× (chroma) excitation filter to remove any stray light. Individual particles identified from the raster scanned image were excited with the same confocal beam until the particles were photobleached. The excitation power was 5.0 μW. Fluorescence emission from single particles was first directed through a 100 μm pinhole to remove any defocused emission and then towards an avalanche photodiode detector (APD). Prior to sending the fluorescence emission to the APD, it was filtered through an ET 542 LP (chroma) filter to remove any leftover excitation light. The APD converted the photons to an electrical signal that was transmitted to a TCSPC module (Picoharp 300) to time stamp the photons. Data analysis was conducted using PicoQuant SymPhoTime 64 software.

Photocatalytic methylene blue degradation

First, 3.0 mL of aqueous solution of each of the fractionated CDs (0.01 mg/mL) was mixed with 300 μL of methylene blue (MB) solution (0.01 mg/mL) in a 4-mL UV/Vis cuvette. Subsequently, 300 μL of 30% H_2O_2 solution was added to the reaction mixture. After 1 min of stirring, the photocatalytic degradation was measured under AM 1.5G simulated solar light illumination (100 mW/cm^2), with a 400 nm cut-off and infrared filter from a 150 W Xe lamp solar simulator (PEC–L01, Peccell Technologies, Inc., Japan). The concentration of MB was determined by UV/vis spectra at 605 nm.

Author Contributions

D.K., M.G., D.Y.K., and B.-S.K. participated in conceiving and designing the project. D.K. contributed to synthesis and characterization of carbon dots and electron transfer process experiment. R.L.C., A.M., N.L.K., C.I.R., and D.Y.K. contributed to ensemble and single-particle analysis. S.-Y.K., W.-J.S., K.Y.H., and H.C. assisted idea development and data interpretation. All authors have given approval to the final version of the manuscript.

Acknowledgements

This work was supported by Samsung GRO project and the National Research Foundation of Korea (NRF-2017M3A7B4052802 and NRF-2018R1 A5 A1025208)

Conflict of Interest

The authors declare no conflict of interest.

Keywords: Carbon nanodots · Surface functional groups · Single-particle spectroscopy · Photoluminescence · Column chromatography

[1] a) X. Michalet, F. F. Pinaud, L. A. Bentolila, J. M. Tsay, S. Doose, J. J. Li, G. Sundaresan, A. M. Wu, S. S. Gambhir, S. Weiss, *Science* **2005**, *307*, 538–544; b) M. Baker, *Nat. Methods* **2010**, *7*, 957–962; c) S. Y. Lim, W. Shen, Z. Gao, *Chem. Soc. Rev.* **2015**, *44*, 362–381.
[2] a) S. N. Baker, G. A. Baker, *Angew. Chem. Int. Ed.* **2010**, *49*, 6726–6744; *Angew. Chem.* **2010**, *122*, 6876–6896; b) J. Lu, J.-x. Yang, J. Wang, A. Lim, S. Wang, K. P. Loh, *ACS Nano* **2009**, *3*, 2367–2375.
[3] a) H. Li, Z. Kang, Y. Liu, S.-T. Lee, *J. Mater. Chem.* **2012**, *22*, 24230–24253; b) Y. Choi, Y. Choi, O.-H. Kwon, B.-S. Kim, *Chem. Asian J.* **2018**, *13*, 586–598.
[4] a) A. P. Demchenko, M. O. Dekaliuk, *Nanoscale* **2016**, *8*, 14057–14069; b) Y. Choi, S. Kim, Y. Choi, J. Song, T.-H. Kwon, O.-H. Kwon, B.-S. Kim, *Adv. Mater.* **2017**, *29*, 1701075; c) S. K. Misra, I. Srivastava, J. S. Khamo, V. V. Krishnamurthy, D. Sar, A. S. Schwartz-Duval, J. A. N. T. Soares, K. Zhang, D. Pan, *Nanoscale* **2018**, *10*, 18510–18519; d) K. Jiang, S. Sun, L. Zhang, Y. Lu, A. Wu, C. Cai, H. Lin, *Angew. Chem. Int. Ed.* **2015**, *54*, 5360–5363; *Angew. Chem.* **2015**, *127*, 5450–5453.
[5] a) S. K. Das, C. M. Luk, W. E. Martin, L. Tang, D. Y. Kim, S. P. Lau, C. I. Richards, *J. Phys. Chem. C* **2015**, *119*, 17988–17994; b) H. Ding, S.-B. Yu, J.-S. Wei, H.-M. Xiong, *ACS Nano* **2016**, *10*, 484–491; c) K. Holá, M. Sudolská, S. Kalytchuk, D. Nachtigallová, A. L. Rogach, M. Otyepka, R. Zbořil, *ACS Nano* **2017**, *11*, 12402–12410; d) Y. Choi, B. Kang, J. Lee, S. Kim, G. T. Kim, H. Kang, B. R. Lee, H. Kim, S.-H. Shim, G. Lee, O.-H. Kwon, B.-S. Kim, *Chem. Mater.* **2016**, *28*, 6840–6847; e) L. Li, T. Dong, *J. Mater. Chem. C* **2018**, *6*, 7944–7970; f) G. E. LeCroy, F. Messina, A. Sciortino, C. E. Bunker, P. Wang, K. A. S. Fernando, Y.-P. Sun, *J. Phys. Chem. C* **2017**, *121*, 28180–28186.
[6] a) B. Ju, H. Nie, Z. Liu, H. Xu, M. Li, C. Wu, H. Wang, S. X.-A. Zhang, *Nanoscale* **2017**, *9*, 13326–13333; b) S. Khan, A. Gupta, N. C. Verma, C. K. Nandi, *Nano Lett.* **2015**, *15*, 8300–8305.
[7] a) Q. Xu, Q. Zhou, Z. Hua, Q. Xue, C. Zhang, X. Wang, D. Pan, M. Xiao, *ACS Nano* **2013**, *7*, 10654–10661; b) H. A. Nguyen, I. Srivastava, D. Pan, M. Gruebele, *ACS Nano* **2020**, *14*, 6127–6137; c) A. M. Chizhik, S. Stein, M. O. Dekaliuk, C. Battle, W. Li, A. Huss, M. Platen, I. A. T. Schaap, I. Gregor, A. P. Demchenko, C. F. Schmidt, J. Enderlein, A. I. Chizhik, *Nano Lett.* **2016**, *16*, 237–242.
[8] D. Bhattacharya, M. K. Mishra, G. De, *J. Phys. Chem. C* **2017**, *121*, 28106–28116.
[9] S. K. Das, Y. Liu, S. Yeom, D. Y. Kim, C. I. Richards, *Nano Lett.* **2014**, *14*, 620–625.
[10] X. Wang, L. Cao, F. Lu, M. J. Meziani, H. Li, G. Qi, B. Zhou, B. A. Harruff, F. Kermarrec, Y.-P. Sun, *Chem. Commun.* **2009**, 3774–3776.
[11] S. Khan, N. C. Verma, A. Gupta, C. K. Nandi, *Sci. Rep.* **2015**, *5*, 11423.
[12] a) Q. Li, M. Zhou, Q. Yang, Q. Wu, J. Shi, A. Gong, M. Yang, *Chem. Mater.* **2016**, *28*, 8221–8227; b) H. Wang, S. Jiang, W. Liu, X. Zhang, Q. Zhang, Y. Luo, Y. Xie, *Angew. Chem. Int. Ed.* **2020**, *59*, 11093–11100; *Angew. Chem.* **2020**, *132*, 11186–11193.
[13] a) Y. Zhang, X. Liu, Y. Fan, X. Guo, L. Zhou, Y. Lv, J. Lin, *Nanoscale* **2016**, *8*, 15281–15287; b) C.-Y. Teng, B.-S. Nguyen, T.-F. Yeh, Y.-L. Lee, S.-J. Chen, H. Teng, *Nanoscale* **2017**, *9*, 8256–8265.
[14] L. Bao, Z.-L. Zhang, Z.-Q. Tian, L. Zhang, C. Liu, Y. Lin, B. Qi, D.-W. Pang, *Adv. Mater.* **2011**, *23*, 5801–5806.
[15] a) L. Wang, S.-J. Zhu, H.-Y. Wang, S.-N. Qu, Y.-L. Zhang, J.-H. Zhang, Q.-D. Chen, H.-L. Xu, W. Han, B. Yang, H.-B. Sun, *ACS Nano* **2014**, *8*, 2541–

2547; b) L. Wang, S.-J. Zhu, H.-Y. Wang, Y.-F. Wang, Y.-W. Hao, J.-H. Zhang, Q.-D. Chen, Y.-L. Zhang, W. Han, B. Yang, H.-B. Sun, *Adv. Opt. Mater.* **2013**, *1*, 264–271.
[16] R. L. Calabro, D.-S. Yang, D. Y. Kim, *J. Colloid Interface Sci.* **2018**, *527*, 132–140.
[17] R. Zondervan, F. Kulzer, S. B. Orlinskii, M. Orrit, *J. Phys. Chem. A* **2003**, *107*, 6770–6776.
[18] T. Gensch, M. Böhmer, P. F. Aramendía, *J. Phys. Chem. A* **2005**, *109*, 6652–6658.
[19] N. Durisic, A. G. Godin, D. Walters, P. Grütter, P. W. Wiseman, C. D. Heyes, *ACS Nano* **2011**, *5*, 9062–9073.
[20] Y. Choi, G. H. Ryu, S. H. Min, B. R. Lee, M. H. Song, Z. Lee, B.-S. Kim, *ACS Nano* **2014**, *8*, 11377–11385.
[21] V. Hinterberger, C. Damm, P. Haines, D. M. Guldi, W. Peukert, *Nanoscale* **2019**, *11*, 8464–8474.
[22] a) Y. Zhou, E. M. Zahran, B. A. Quiroga, J. Perez, K. J. Mintz, Z. Peng, P. Y. Liyanage, R. R. Pandey, C. C. Chusuei, R. M. Leblanc, *Appl. Catal. B* **2019**, *248*, 157–166; b) Z. Zhang, T. Zheng, X. Li, J. Xu, H. Zeng, *Part. Part. Syst. Charact.* **2016**, *33*, 457–472.
[23] a) S. Bhattacharyya, F. Ehrat, P. Urban, R. Teves, R. Wyrwich, M. Döblinger, J. Feldmann, A. S. Urban, J. K. Stolarczyk, *Nat. Commun.* **2017**, *8*, 1401; b) G. S. Das, J. P. Shim, A. Bhatnagar, K. M. Tripathi, T. Kim, *Sci. Rep.* **2019**, *9*, 15084.
[24] Q. Li, S. Wang, Z. Sun, Q. Tang, Y. Liu, L. Wang, H. Wang, Z. Wu, *Nano Res.* **2019**, *12*, 2749–2759.
[25] D. Hong, Y. Choi, J. Ryu, J. Mun, W. Choi, M. Park, Y. Lee, N.-S. Choi, G. Lee, B.-S. Kim, S. Park, *J. Mater. Chem. A* **2019**, *7*, 20325–20334.

Manuscript received: September 17, 2021
Revised manuscript received: November 1, 2021
Accepted manuscript online: November 4, 2021
Version of record online: November 18, 2021